Journal of Applied Polymer Science

Preparation of Highly Thermally Conducting Polyamide 6/Graphite Composites via Low-Temperature *In Situ* Expansion

Shengtai Zhou, Lin Yu, Xin Song, Jin Chang, Huawei Zou, Mei Liang
State Key Laboratory of Polymer Materials Engineering, Polymer Research Institute of Sichuan University, Chengdu 610065, China
Correspondence to: H. Zou (E-mail: hwzou@163.com) and M. Liang (E-mail: liangmeiww@163.com)

ABSTRACT: Highly thermally conducting polyamide 6 (PA6) composites with high loadings of low-temperature expandable graphite (LTEG) were prepared by an *in situ* exfoliation melting process, and the thermal conductivity of the composites was measured by a hot-disk method. A two-point method was applied to evaluate the electrical conductivity of the composites with various graphite loadings, and the thermal percolation was observed in the vicinity of the electrical percolation threshold concentration. Dynamic rheology analysis was used to define the geometric change caused by the interconnection of the *in situ* exfoliated graphite flakes. X-ray diffraction measurement confirmed that the exfoliation of LTEG was crucial to the overall thermal conductivity of the composites. Dynamic mechanical analysis revealed that the incorporation of LTEG significantly improved the damping properties of PA6. Thermogravimetric analysis and differential scanning calorimetry measurements were applied to study the thermal properties of the investigated PA6/LTEG composites. © 2013 Wiley Periodicals, Inc. J. Appl. Polym. Sci. 000: 000–000, 2013

KEYWORDS: composites; conducting polymers; polyamides; thermal properties

Received 8 April 2013; accepted 28 May 2013; Published online
DOI: 10.1002/app.39596

INTRODUCTION

The addition of highly thermally conducting fillers within a polymer matrix is an effective method for developing thermal conductive composites for industrial applications, such as electronics, heat sinks, and heat exchangers.[1,2] Recently, considerable research has been conducted on the processing and characterization of the composites with graphitic fillers to improve the mechanical, thermal, electrical, and gas-barrier properties of polymers.[3–10]

Graphite, a naturally abundant layered material, consists of a structure where carbon atoms are bound by covalent bonds to other carbons in the same plane, and stacks of graphite flakes, known as *graphene*, are weakly bonded to each other by van der Waal's forces; this makes the intercalation of inserting agents possible.[9,11] The superior properties, such as excellent conductive properties, generated from the two-dimensional graphene sheets make graphite an excellent candidate for thermal and electrical management systems, which could be used in many areas where a high thermal dissipation and conductivity are required.[8,12] Graphite intercalation compound, which denotes expandable graphite (EG), is prepared by the intercalation of a variety of intercalation agents[13,14] and can be rapidly exfoliated, to some extent, hundreds of times over its initial volume when subjected to high temperature to form a wormlike morphology. Therefore, EG is widely used as a flame-retardant additive in polyurethane foams[15,16] and polymer-based composites[17,18] because of its intumescent nature. However, the exfoliation process of EG also makes it easier to form three-dimensional conductive pathways[8] that enhance the conductive properties of EG-containing composites by optimizing the filler distribution in the polymer matrix; this is crucial to the overall thermal conductivity of the composites. The expanded graphite exhibits a layered structure similar to layered silicates and has a good affinity with polymers;[12,19] this structure can be obtained from EG with *in situ* melt blending to form continuous thermal conductive pathways.[8] A consensus has been reached that the formation of heat conduction pathways and the stacking density of conductive fillers in the composites are both important factors that contribute to the overall thermal conductivity of the composites.[20] Moreover, the incorporation of EG or expanded/exfoliated graphite into the polymer matrix to obtain conductive composites is not a novel idea.[8,21–24] However, to the best of our knowledge, the introduction of EG, which has a lower expanded temperature, has rarely been reported.

In this study, a commercial-grade low-temperature expandable graphite (LTEG) was introduced into polyamide 6 (PA6) to prepare highly thermally conducting composites. The expanded/exfoliated structure was observed during the fabrication process of the PA6/LTEG composites; this was due to the fact that the processing

temperature (240°C) was higher than the initial expanded temperature, that is, 150°C, for LTEG. We believe that EG owned a low initial expandable temperature and was highly expanded during the fabrication process of the PA6/LTEG composites. The effect of the loading fractions of LTEG on the morphology and properties, including the thermal, electrical, and crystalline properties and viscoelastic behavior, of the composites is also reported.

EXPERIMENTAL

Materials

PA6 (Ultramid B3S), with a melt volume-flow rate of 175 cm^3/10 min (275°C, 5 kg) and a density of 1.13 g/cm^3, was purchased from BASF Chemical Co. (Germany). LTEG, with the trademark ADT KP801, was obtained from Shijiazhuang ADT Carbonic Material Factory (China). The sulfur-free EG was a kind of graphite intercalation compound and was prepared by the intercalation of acetic acid. The initial expanded temperature for LTEG was in the vicinity of 150°C, and the expansion ratio was 230 mL/g. LTEG exhibited a particle size of nearly 180 μm with a density 2.20 g/cm^3 and was used as a thermally conductive filler as it was received. All of the property data were provided by the manufactures.

Sample Preparation

A Brabender internal mixer (Duisburg, Germany), equipped with contrarotating blades, was used to prepare the thermally conducting composites. PA6 was blended with various percentages of LTEG. Before blending, the PA6 pellets were dried *in vacuo* at 85°C for 10 h. The preparation process for the PA6 blends containing 5, 10, 15, 20, 25, 30, 35, 40, 50, and 60 wt % of LTEG was carried out at 30 rpm for 10 min at 20°C above the polymer matrix melting temperature, that is, 240°C. These blends were called EG5, EG10, EG15, EG20, EG25, EG30, EG35, EG40, EG50, and EG60, respectively. Predetermined shaped specimens were prepared by hot pressing (10 MPa, 240°C) and were then subsequently used for different measurements.

Characterization

Thermal Conductivity Measurements. The thermal conductivity measurement of the composites was carried out by a thermal constant analyzer (Hot Disk TPS 2500, Sweden) at a certain electrical power exerted on the samples for a corresponding measuring time. The hot-disk sensor was placed between two pieces of prepared samples, and the whole unit was clamped tightly. The sensor acted as both a heat source and a temperature sensor. The experimental data of both samples were collected at the same time, and the reported thermal conductivity was the average value of both samples.

Electrical Conductivity (σ) Measurements. The specimens used for the resistivity measurement were prepared with dimensions of 100 × 10 × 1 mm^3. Contact resistances were minimized with silver paint at the probe/sample interface. The volume resistivity [ρ (Ω m)] was determined by a two-probe method[25] with a Keithley 6487 picoammeter and then converted into σ (S/m) with eq. (1):

$$\sigma = \frac{1}{\rho} = \frac{L}{RS} \tag{1}$$

where L is the distance between clumps (m), R is the electrical resistance (Ω), and S is the cross-sectional area (m^2).

Morphology of the PA6/LTEG Composites. The morphology of the composites was observed by scanning electron microscopy (SEM; JSM-5900, JEOL, Tokyo, Japan) with an acceleration voltage of 5 kV. The samples were cryogenically fractured in liquid nitrogen, and all of the fractured surfaces were coated with gold to enhance the image resolution and to prevent electrostatic charging.

Differential Scanning Calorimetry (DSC). The melting and crystallization behaviors of the composites were determined with a differential scanning calorimeter (DSC-204, Netzsch, Germany). Experiments were performed with 6–10-mg samples under dry nitrogen gas conditions. First, the sample was quickly heated to 250°C and held at 250°C for 5 min to erase the thermal history. Subsequently, the sample was cooled at a rate of 10°C/min to 50°C and held at 50°C for 5 min. It was then scanned from 50 to 250°C at a heating rate of 10°C/min. The crystallinity (X_c) of the composites was calculated with eq. (2):

$$X_c = \frac{\Delta H_f}{\Delta H_f^m \chi_A} \tag{2}$$

where ΔH_f is the melting enthalpy of PA6 for the composites, ΔH_f^m is the enthalpy of the polymer with an X_c of 100%, and the literature value of 230 J/g[26] for the 100% crystalline PA6 was used. χ_A denotes the fraction of PA6 in the composites.

Dynamic Rheological Tests. The viscoelastic behavior of the samples was analyzed with the help of a dynamic rheometer (Bohlin Gemini 2000, Malvern, British) in the melt state. The samples were studied under a constant-strain mode. To keep the response in the linear viscoelastic region, the applied strain was set at 1%.[27] The samples were prepared in a parallel-plate form with a diameter of 25 mm and a thickness of 1 mm, and the rheological tests were performed at 250°C with a gap distance of about 1 mm under a nitrogen atmosphere. All of the samples were tested in frequency sweep ranges from 0.01 to 100 Hz. The storage modulus (G'), loss modulus (G''), and complex viscosity (η^*) of all of the samples were recorded as a function of angular frequency (ω).

X-ray Diffraction (XRD) Analysis. XRD scans of the LTEG powder, PA6, and PA6/LTEG composite plates were carried out on a D/MAX-III X-ray diffractometer (DY1291, Philips, Holland) with Cu Kα radiation ($K = 0.1542$ nm, where K is the wavelength of X-ray) at a generator voltage of 40 kV and a generator current of 35 mA. The scanning speed was 9°/min, and the step size was 0.03° from 1.5 to 30°.

Thermogravimetric Analysis (TGA). TGA was conducted on a thermogravimetric analyzer (TG 209F1 Iris, Netzsch, Germany) under dry nitrogen gas with a flow rate of 60 mL/min. The samples were heated at a rate of 10°C/min, and the relative mass loss of the samples was recorded from 30 to 800°C.

Dynamic Mechanical Analysis (DMA). Dynamic mechanical experiment was performed at 1 Hz with a heating rate of 3°C/min from −100 to 180°C with the Izod mode with a TA Instruments Q800 apparatus. Samples with a size of 30 × 10 × 4 mm^3 and prepared by hot press-molding were cooled quickly down to −100°C with liquid nitrogen and allowed to

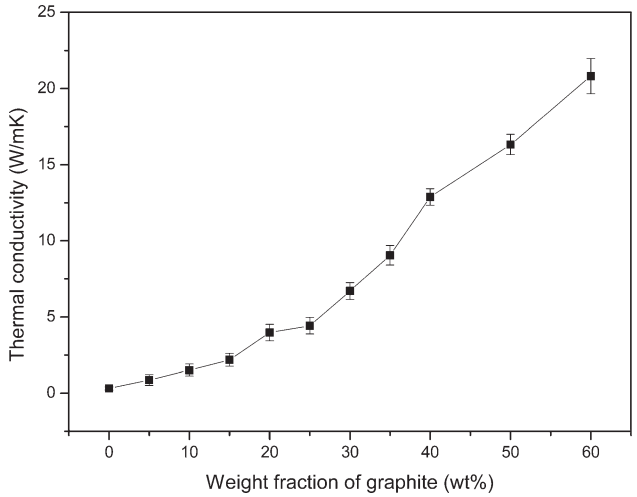

Figure 1. Thermal conductivity of the PA6/LTEG composites as a function of the graphite content.

equilibrate at −100°C for 5 min before the measurements. The peak temperature of the loss factor (tan δ) was regarded as the glass-transition temperature (T_g) of the sample.

RESULTS AND DISCUSSION

Thermal Conductivity of the PA6/LTEG Composites

The effect of the loading concentrations of LTEG on the thermal conductivity of the PA6/LTEG composites is shown in Figure 1. The thermal conductivity always increased with increasing weight fraction of LTEG up to 60 wt %. The thermal conductivity of the filled PA6 increased slowly with LTEG loading when it was less than 15 wt %; at loadings greater than 15 wt %, the thermal conductivity increased quickly. The thermal conductivity of PA6 filled with 60 wt % LTEG reached 21.05 versus 0.2939 W m^{-1} K^{-1} for the virgin PA6 matrix. The thermal conductivity of the composites increased slowly at low loadings, and this was mainly ascribed to the inadequate formation of the thermally conducting networks by heat-conductive fillers and the high thermal resistance generated from the polymer matrix. As the filler concentration increased, the high expansion ratio of LTEG during the *in situ* expanding process led to the formation of thermally conductive networks,[8] and a more compact filler packing structure was achieved with increasing loading of LTEG; this was also a crucial factor in the overall thermal conductivity of the composites.

When the filler loading further increased from 40 to 60 wt %, the thermal conductivity increased almost linearly again with a minor slope. With increasing filler loading, the number of the newly formed thermally conductive networks no longer played a vital role in enhancing the thermal conductivity, whereas the packing structure of the filler and void defects introduced during the exfoliation process became the main factors that impaired the overall thermal conductivity of the PA6/LTEG composites. In light of these factors, the thermal conductivity increased rather slowly at high loading fractions.

σ

Like most polymers, PA6 used for the matrix material was not electrically conductive and its room temperature ρ in a dry state was as high as 10^{15} Ω cm (according to the B3S datasheet). The log σ values are plotted against the weight fractions of LTEG in Figure 2. It is shown that σ of the LTEG-filled polymers increased with increasing graphite concentration. The addition of graphite significantly enhanced the conductivity of PA6, with a sharp transition from a typical electrical insulator to an electrical semiconductor. At 5 wt % LTEG, the conductivity of the polymer composite was almost five orders of magnitudes higher than that of the virgin PA6 matrix. At 15 wt % LTEG, the augmentation of the σ improved slowly; this was ascribed to the good dispersion of LTEG within the polymer and the formation of conductive networks by the *in situ* exfoliated graphite flakes. Moreover, Figure 2 indicates that the percolation threshold was observed near 15 wt % LTEG. The increase in σ for the PA6 composites above 15 wt % LTEG was mainly due to the increasing number of interconnecting networks formed by the *in situ* exfoliated graphite flakes and the more compact structures rendered by the conductive filler.

Morphology

Figure 3 shows the SEM micrographs of LTEG at different magnifications. The representative micrograph in Figure 3(b) shows that LTEG consisted of a few layers of graphite flakes. The morphology of the cryofractured surfaces of the composites is shown in Figure 4. LTEG was evenly dispersed in PA6 matrix and exfoliated well during the melt blending process. Specifically, it is shown in Figure 4(c) that the *in situ* exfoliated graphite flakes nearly formed the conductive networks in the composite blend and contributed to a rapid growth of thermal conductivity in the system. Moreover, a rather high thermal conductivity (2.257 W m^{-1} K^{-1}) was achieved at 15 wt % LTEG; this was nearly eight times higher than that of the virgin PA6 matrix. Figure 4(d) shows that the graphite flakes already formed perfect thermally conductive networks, and a more compact filler structure was obtained with increasing LTEG content in the composite blend because of the *in situ* exfoliation of LTEG. Both elements were crucial to the overall thermal conductivity of the composites. The thermal conductivity of the

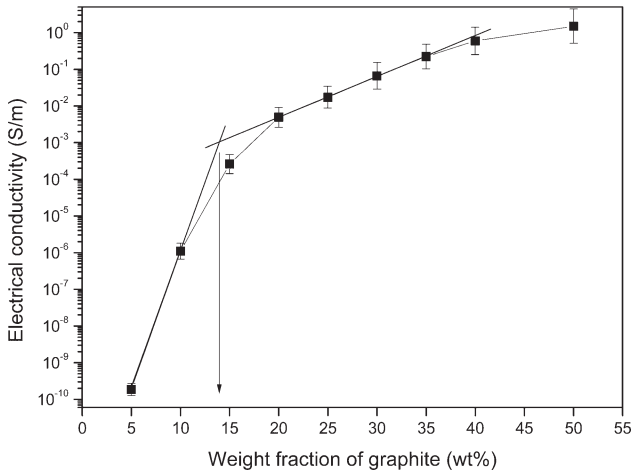

Figure 2. σ of the PA6/LTEG composites as a function of the LTEG content.

Applied Polymer SCIENCE

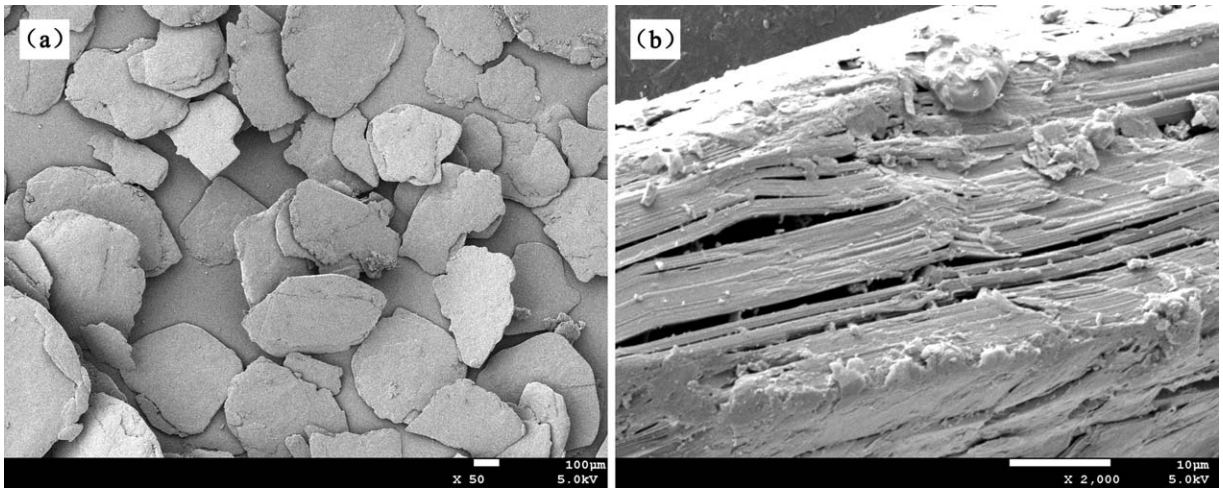

Figure 3. SEM micrographs of EG at different magnifications: (a) 50 and (b) 2000×.

composites with higher filler loadings increased rapidly and reached 21.05 W m^{-1} K^{-1} at 60 wt % LTEG; this was approximately 72 times higher than that of the virgin PA6.

DSC

Figure 5 shows the reheating and cooling DSC curves of the virgin PA6 and PA6/LTEG blend composites. For clarity, all of the DSC scan curves shown here were shifted vertically. Table I shows the observed ΔH_f and X_c values for PA6.

As shown in Figure 5(a), all of the samples exhibited a main strong melting peak (ca. 220°C) and a weak melting peak (ca. 215°C). The melting peak at about 220°C was consistent with the melting temperature of the α-form crystal of PA6. In

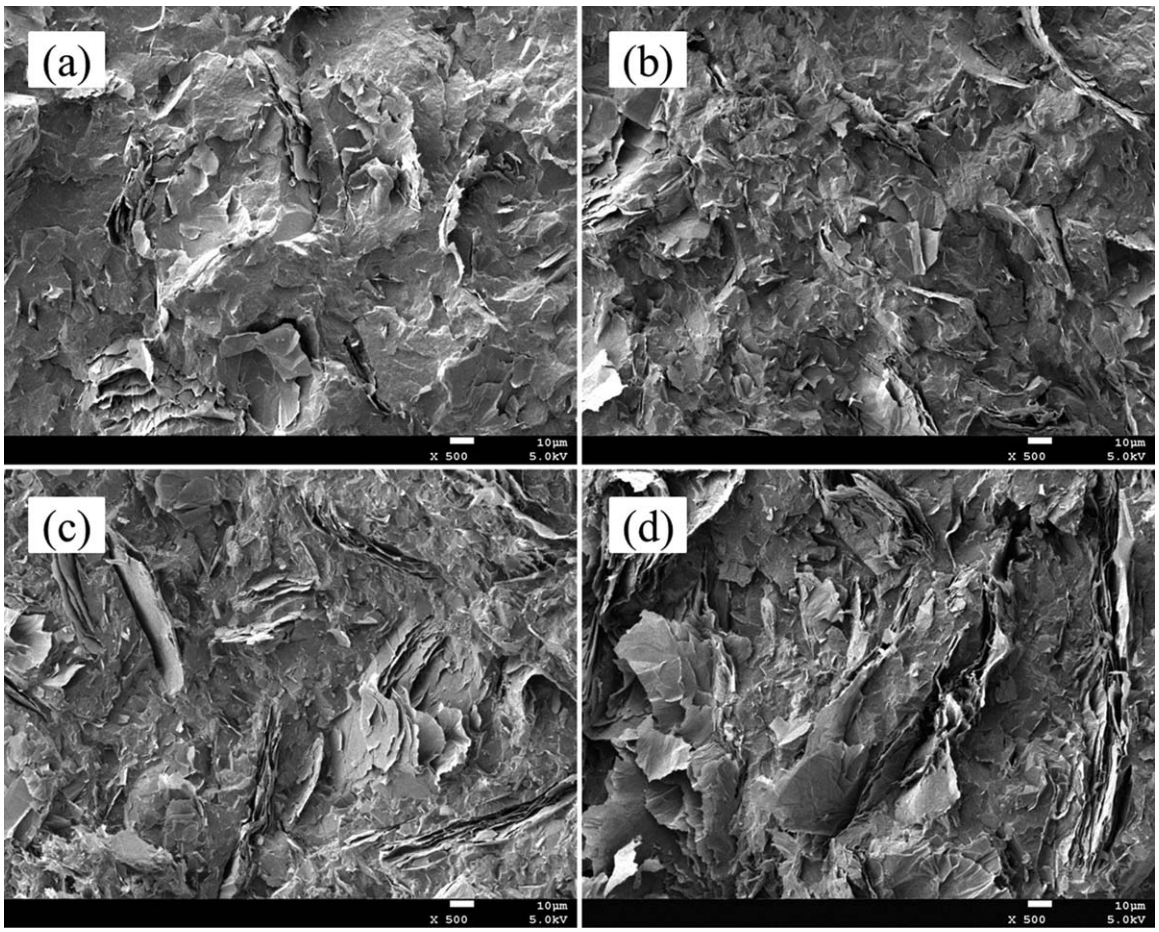

Figure 4. SEM images of the cryofractured surfaces of the PA6/LTEG composite: the morphology of (a) EG5, (b) EG10, (c) EG15, and (d) EG20.

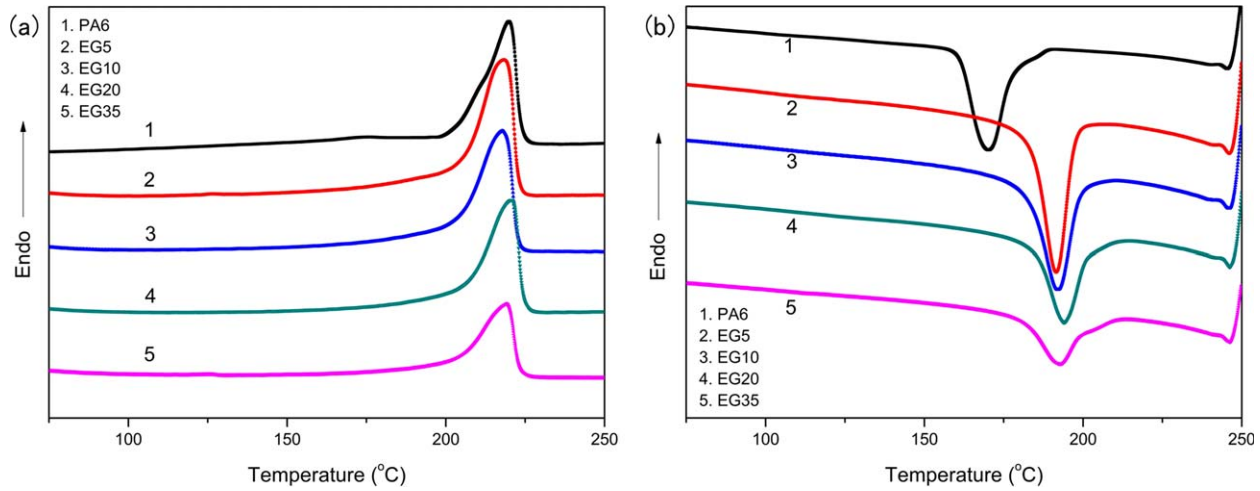

Figure 5. (a) DSC reheating and (b) DSC cooling curves for the PA6/LTEG blends. [Color figure can be viewed in the online issue, which is available at wileyonlinelibrary.com.]

addition, the weak peak at about 215°C corresponded to the melting temperature of the γ-form crystal of PA6.[28,29] It is illustrated in Table I that the incorporation of LTEG greatly affected X_c of the PA6 matrix. An increased X_c was observed for composites with relatively lower LTEG loading fractions. This suggested that the exfoliated graphite flakes offered crystallization sites, which aided the formation of PA6 crystals and led to an improvement in X_c. However, further increases in the LTEG concentrations resulted in a decrease in the degree of X_c for PA6; this could be explained by the fact that the presence of exfoliated graphite flakes hindered the formation of large crystalline domains, which resulted from the limited space and confinement effect that were imposed on the PA6 chains by the large number of flake platelets.[29,30] Interestingly, a weakness of the shoulder peak was evident in Figure 5(a); we considered that the introduced LTEG had a suppression effect on the formation of the γ-crystalline form for the PA6.

Unlike the melting behavior of the composites, the crystallization process was greatly affected by the introduction of LTEG into the PA6 matrix. For PA6/LTEG blends, it was easy to see that graphite played the role of nucleating agent[31–33] and accelerated the crystallization process at higher temperatures for the PA6 matrix.

Dynamic Rheological Analysis

The dependence of G', G'', and η^* on ω for the PA6/LTEG composites is shown in log–log plots in Figure 6. The modulus value of the composites increased with increasing LTEG content in the range of frequency that we used. It was clear that both G' and G'' were sensitive enough to be used to evaluate the rheological behavior of the samples, depending on the structural changes in the composites. With G' versus ω taken as an example, the magnitude of the G' increased and the slopes of the curves decreased in the low-frequency region with increasing filler content. Particularly, starting from 15 wt % LTEG, a plateau was observed at low frequencies in G', and a pronounced shear-thinning behavior was noticeable in η^*. This relationship is a well-known phenomenon for composites, which indicates a physical network formation by the inorganic fillers.[34,35] The *in situ* exfoliation of LTEG during the sample preparation process was believed to be responsible for the observed structural changes in the composites.

Table I. ΔH_f and X_c Values for the PA6 Matrix

Sample ID	LTEG (wt %)	ΔH_f (J/g)	X_c
PA6	0	99.33	0.432
EG5	5	106.6	0.488
EG10	10	99.14	0.479
EG20	20	83.79	0.455
EG35	35	60.03	0.402

The identification of the percolation concentration could be performed with this figure with the rheological data. As shown in Figure 6(a), a change in the frequency dependence was notable at various LTEG concentrations; it was particularly noticeable in the range between 10 and 15 wt %. Above this particular concentration, the rheological behavior changed from a viscous fluid to an elastic solid; this indicated the good construction of a thermally conducting network by the exfoliated graphite flakes, that is, the percolation threshold. The transition was observed at exactly the same composition as in the plots of G'' and η^* versus frequency. In combination with the thermal and σ results, we concluded that thermal conductive networks were formed near 15 wt % LTEG or, more specifically, between 10 and 15 wt %; this enhanced the thermal conductivity and σ of the composites.

XRD Characterization

XRD experiments were carried out to investigate the crystal structure behavior of the composites. For comparison, the XRD patterns of the virgin PA6 and LTEG are illustrated in Figure 7. The characteristic peak observed at $2\theta = 26.5°$ belonged to the crystalline form of the stacked graphite flakes,[36] whereas the slight increase in the slope before 26° may have been due to

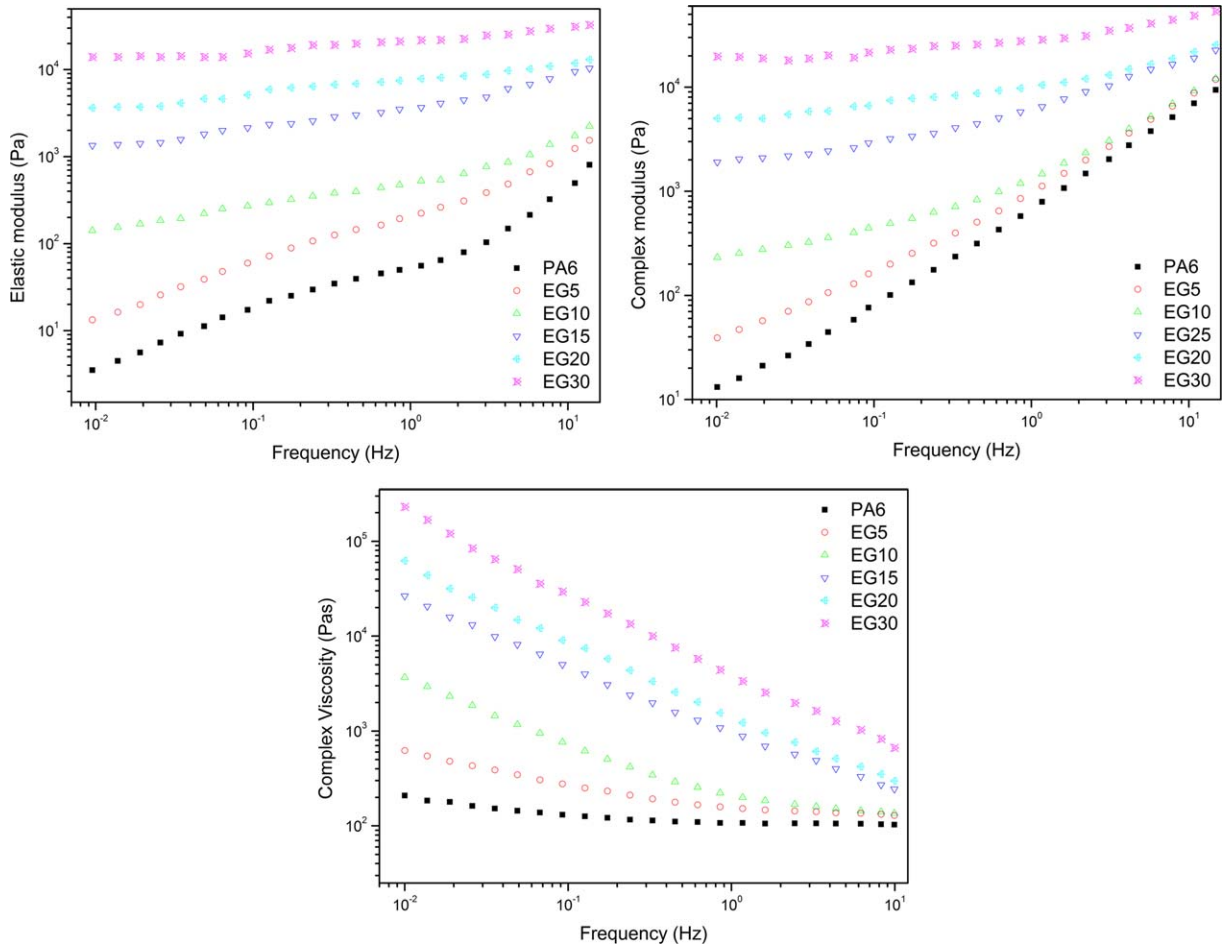

Figure 6. (a) G', (b) G'', and (c) η^* as a function of the angular frequency for different LTEG contents for the PA6/LTEG composites at 250°C. [Color figure can be viewed in the online issue, which is available at wileyonlinelibrary.com.]

the intercalation of the inserting agents, which enlarged the layer space between the graphite flakes. PA6 is known to have two different crystalline forms, namely, α and γ forms. The formation of these two forms is influenced by the crystallization conditions and the presence of fillers.[29,37] Figure 8 shows the XRD patterns for the LTEG-containing composites at various loading fractions. The inset pictures are the magnified versions, mainly for the PA6 matrix. All of the blended examples showed two peaks, which were located at $2\theta = 20°$ and 23.5°, that were characteristic of the α-crystalline form of PA6 and a peak located at $2\theta = 21.5°$ that corresponded to the γ-crystalline form of PA6.[37] However, the characteristic peak appearing at $2\theta = 26.5°$ was attributed to the crystalline form and was derived from the *in situ* exfoliated graphite flakes. It is clear that the addition of LTEG to PA6 resulted in significant changes in the proportion of the α-/γ-crystalline forms of PA6. As shown in Figure 7, the virgin PA6 exhibited predominantly the γ-crystalline form, whereas the PA6/LTEG composites showed much a higher α-crystalline form of PA6. This means that the presence of LTEG induced the formation of the α-crystalline form of PA6; this was probably because the exfoliated graphite flakes could act as nucleation sites for the PA6 chains. A similar result was reported for a PA6/polypropylene (PP)/multi-walled carbon nanotube (MWNT) system.[30] The same results were also observed from the DSC reheating thermograms for the shoulder peak at 215°C; this corresponded to the γ-crystalline form of PA6, which decreased with the incorporation of LTEG. The exfoliated graphite flakes maintained good crystalline forms in the PA6/LTEG composites; this could be deduced from the XRD

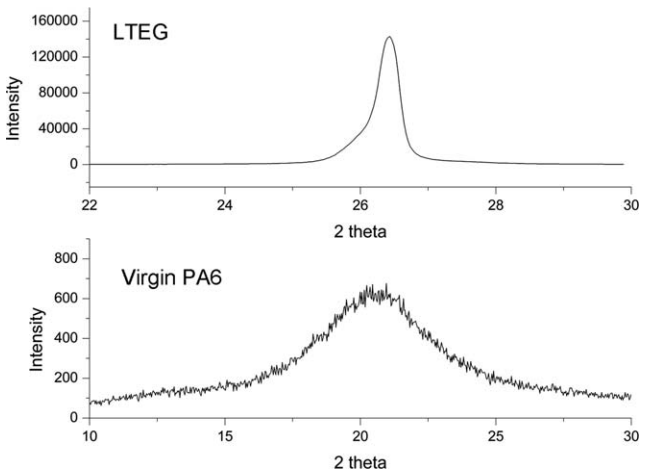

Figure 7. XRD patterns of LTEG and virgin PA6.

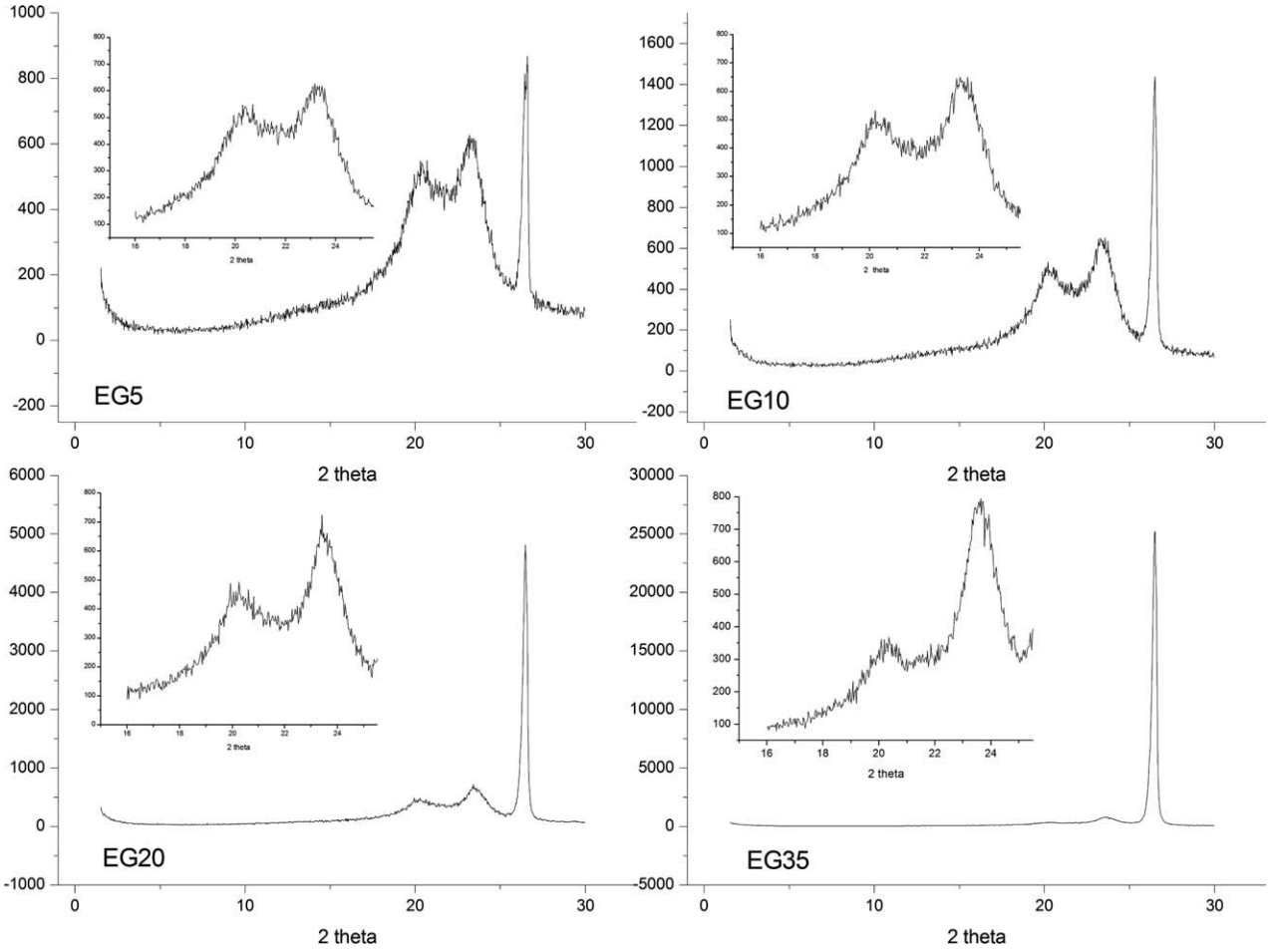

Figure 8. XRD comparison patterns for the various PA6/LTEG composites.

patterns of the composites, for the intensity value of the characteristic peak formed by the *in situ* exfoliated graphite flakes increased remarkably with increasing LTEG loading content. This was crucial to the overall thermal conductivity of the composites.

Thermal Stability Analysis

The TGA and derivative thermogravimetry (DTG) thermograms as a function of the temperature are shown in Figure 9. The representative thermal analysis data of the samples are listed in Table II. The initial decomposition temperature (T_d) was the

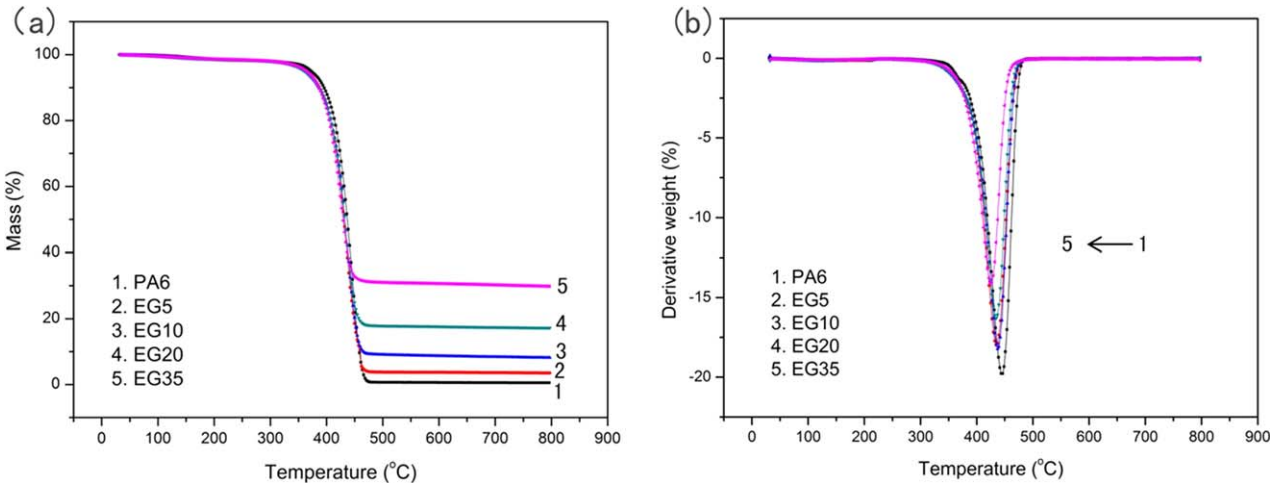

Figure 9. TGA and DTG thermograms of the virgin PA6 and PA6/LTEG blends. [Color figure can be viewed in the online issue, which is available at wileyonlinelibrary.com.]

Table II. TGA T_d, T_{max}, and R_{800} Values of the Virgin PA6 and PA6/LTLG Blends

Sample	T_d (°C)	T_{max} (°C)	R_{800} (%)
Virgin PA6	370.8	436.8	0.52
EG5	363.4	435.6	3.52
EG10	361.5	437.6	8.15
EG20	360.7	434.6	17.2
EG35	361.4	425.4	29.8

temperature at 5% weight loss, whereas the maximum weight loss temperature (T_{max}) was taken from the peak value of the DTA thermograms. The thermograms show that there was only one decomposition stage in the heating process, and T_d decreased as the LTEG increased (Table II). This indicated that the thermal stability of the composites deteriorated with the addition of LTEG into the PA6 matrix; this was in contrast to polylactide/exfoliated graphite nanocomposites.[38] However, T_{max} changed marginally, and a much higher residual weight percentage at 800°C (R_{800}) was obtained for EG5. This could be ascribed to the barrier effect of the exfoliated graphite flakes against the volatile pyrolyzed products in the matrix, which retarded the thermal degradation of the composites.[39] Interestingly, T_{max} decreased significantly with increasing loading of LTEG in the composites; for example, its value was nearly 10°C lower for EG35 than for EG5. The most probable reasons for this were as follows: (1) the *in situ* exfoliation of LTEG introduced a certain number of void defects, which could be confirmed by the SEM observations, and thus accelerated the degradation process, and (2) the high thermal conductivity of the composites facilitated the heat conduction process into the internal regions of the PA6/LTEG composites, and then, degradation could occur simultaneously inside and outside the composites.

DMA

DMA is an efficient tool for evaluating the viscoelastic properties and obtaining information about the microstructure of blend composites. G', G'', and tan δ for a series of PA6/LTEG composites are shown as a function of temperature in Figure 10. As shown in Figure 10(a), the magnitude of G' of the typical PA6 and PA6/LTEG composites decreased linearly with temperature in the glass-transmission region, and its value increased

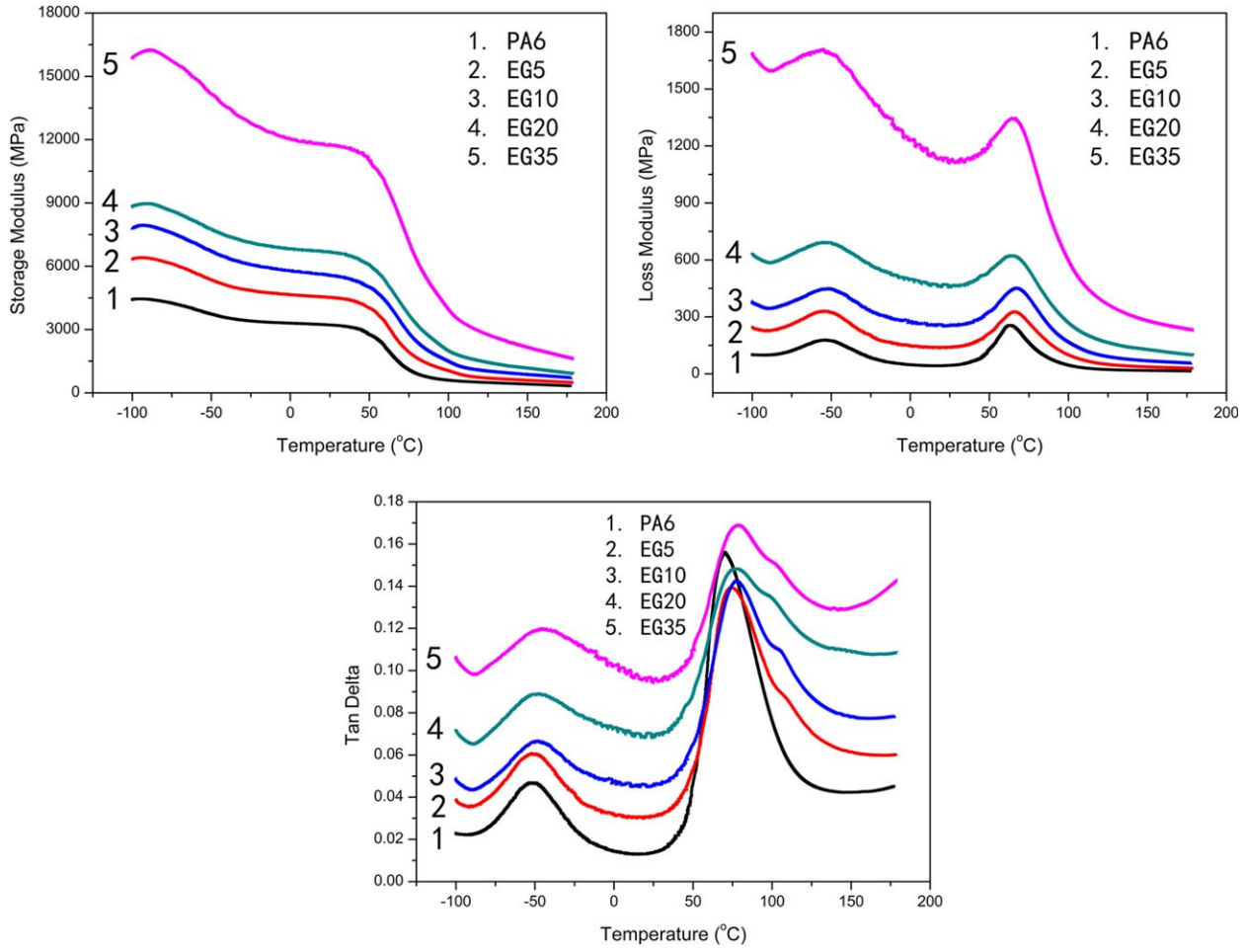

Figure 10. DMA spectra of PA6 with different LTEG loading fractions: (a) G', (b) G'', and (c) tan δ. [Color figure can be viewed in the online issue, which is available at wileyonlinelibrary.com.]

significantly with incremental LTEG loading fraction in the composites. A similar trend of the value of the modulus was observed in the melt rheology analysis. As shown in Figure 10(b,c), there were two transition peaks for the G'' and tan δ curves; these corresponded to the α relaxation for the chain segmental motion of the macromolecules, which can be generally designated as T_g, and the β relaxation resulting from the motion of units that were smaller than the chain segments.[40] In this study, the PA6/LTEG composites showed a consistently higher G'' over that of the virgin PA6 matrix, which increased with the concentration of graphite. The increase in the modulus may have been due to the incorporation of LTEG, and the *in situ* exfoliated graphite flakes had an enhancement effect on the PA6 matrix. Moreover, the interconnection of the exfoliated graphite flakes was also considered to be the main influencing factor.

DMA also revealed that the addition of LTEG had a pronounced effect on the viscoelastic behavior of the composites. As shown in Figure 10(c), T_g of PA6 increased slightly with the incorporation of LTEG. The T_g's were about 70, 74, 77, 78, and 80°C for the virgin PA6, EG5, EG10, EG20, and EG35, respectively. Specifically, the increase of T_g was believed to be the confinement effect of the *in situ* exfoliation graphite flakes, which could restrict the segmental motion of the polymer chains.[41] The improvement of the viscoelastic properties was mainly due to the existing internal friction[42] between the polymer matrix and the added graphite and between the graphite flakes; this was beneficial to the dissipation of energy and thus increased the damping properties of the obtained composites.

CONCLUSIONS

In this study, very highly thermally conducting composites were achieved via an *in situ* exfoliation process of LTEG-filled PA6 during melt blending. A thermal conductivity of 21.05 W m^{-1} K^{-1} was achieved for the PA6/LTEG composite at its maximum filler loading of 60 wt %; this conductivity was approximately 72 times higher than that of the virgin PA6. In the presence of LTEG, a thermal conductivity increase and a percolation threshold reduction for the PA6/LTEG composites were achieved simultaneously. The *in situ* expansion process of LTEG, which formed three-dimensional connected networks, was thought to be the crucial factor in the enhancement of the conductive properties of the composites. Dynamic rheology tests confirmed network formation by the *in situ* exfoliated graphite flakes in the polymer matrix; this conformed to the SEM observations. DMA revealed that the incorporation of LTEG had a pronounced effect on the viscoelastic properties of the composites; this was thought to be the influence of the existing internal friction between the PA6 matrix and graphite flakes and between graphite flakes.

ACKNOWLEDGMENTS

The authors thank the National Natural Science Foundation of China (contract grant number 51273118) and the Science and Technology Pillar Program of Sichuan (contract grant number 2013FZ0006) for their financial support and the Analytical and Testing Center of Sichuan University for SEM observations.

REFERENCES

1. Zhou, W.; Wang, C.; Ai, T.; Wu, K.; Zhao, F.; Gu, H. *Compos. A* **2009**, *40*, 830.
2. Han, Z.; Fina, A. *Prog. Polym. Sci.* **2011**, *36*, 914.
3. Debelak, B.; Lafdi, K. *Carbon* **2007**, *45*, 1727.
4. Chen, D.; Chen, G. *J. Reinf. Plast. Compos.* **2011**, *30*, 757.
5. Fukushima, H.; Drzal, L. T.; Rook, B. P.; Rich, M. J. *J. Therm. Anal. Calorim.* **2006**, *85*, 235.
6. Uhl, F. M.; Yao, Q.; Nakajima, H.; Manias, E.; Wilkie, C. A. *Polym. Degrad. Stab.* **2005**, *89*, 70.
7. George, J. J.; Bandyopadhyay, A.; Bhowmick, A. K. *J. Appl. Polym. Sci.* **2008**, *108*, 1603.
8. Kim, S. R.; Poostforush, M.; Kim, J. H.; Lee, S. G. *Express Polym. Lett.* **2012**, *6*, 476.
9. Lee, Y.; Kim, D.; Seo, J.; Han, H.; Khan, S. B. *Polym. Int.* **2013**, DOI 10.1002/pi.4434.
10. Tu, H.; Ye, L. *Polym. Adv. Technol.* **2009**, *20*, 21.
11. Uhl, F. M.; Yao, Q.; Wilkie, C. A. *Polym. Adv. Technol.* **2005**, *16*, 533.
12. Sengupta, R.; Bhattacharya, M.; Bandyopadhyay, S.; Bhowmick, A. K. *Prog. Polym. Sci.* **2011**, *36*, 638.
13. Dresselhaus, M. S.; Dresselhaus, G. *Adv. Phys.* **1981**, *30*, 139.
14. Li, J.; Feng, L.; Jia, Z. *Mater. Lett.* **2006**, *60*, 746.
15. Chattopadhyay, D. K.; Webster, D. C. *Prog. Polym. Sci.* **2009**, *34*, 1068.
16. Modesti, M.; Lorenzetti, A.; Simioni, F.; Camino, G. *Polym. Degrad. Stab.* **2002**, *77*, 195.
17. Chung, D. D. L. *J. Mater. Sci.* **1987**, *22*, 4190.
18. Wang, J. Q.; Chow, W. K. *J. Appl. Polym. Sci.* **2005**, *97*, 366.
19. Li, Y.; Chen, G. *Polym. Eng. Sci.* **2007**, *47*, 882.
20. Ishida, H.; Rimdusit, S. *Thermochim. Acta* **1998**, *32*, 177.
21. He, F.; Lau, S.; Chan, H. L.; Fan, J. *Adv. Mater.* **2009**, *21*, 710.
22. Zhang, X.; Liang, G.; Chang, J.; Gu, A.; Yuan, L.; Zhang, W. *Carbon* **2012**, *50*, 4995.
23. Zhang, W.; Wong, S. C. *Compos. Sci. Technol.* **2003**, *63*, 225.
24. Li, J.; Xu, Y.; Li, M.; Mi, C.; Li, J. *J. Low Temp. Phys.* **2010**, *160*, 240.
25. Antar, Z.; Feller, J. F.; Noël, H.; Glouannec, P.; Elleuch, K. *Mater. Lett.* **2012**, *67*, 210.
26. Wei, Q.; Chionna, D.; Galoppini, E.; Pracella, M. *Macromol. Chem. Phys.* **2003**, *204*, 1123.
27. Chen, Y.; Zou, H.; Liang, M.; Liu, P. *J. Appl. Polym. Sci.* **2013**, *129*, 945.
28. Wahit, M. U.; Hassan, A.; Ishak, Z. A. M.; Rahmat, A. R.; Bakar, A. A. *J. Thermoplast. Compos.* **2006**, *19*, 545.
29. Kusmono; Ishak, Z. A. M.; Chow, W. S.; Takeichi, T.; *Rochmadi. Eur. Polym. J.* **2008**, *44*, 1023.
30. Zhang, L.; Wan, C.; Zhang, Y. *Polym. Eng. Sci.* **2009**, *49*, 1909.
31. Zheng, W.; Lu, X.; Wong, S. C. *J. Appl. Polym. Sci.* **2004**, *91*, 2781.

32. Sorrentino, L.; Aurilia, M.; Cafiero, L.; Cioffi, S.; Iannace, S. *J. Cell. Plast.* **2012**, *48*, 355.

33. Cerezo, F. T.; Preston, C. M. L.; Shanks, R. A. *Macromol. Mater. Eng.* **2007**, *292*, 155.

34. Kasgoz, A.; Akın, D.; Durmus, A. *Polym. Eng. Sci.* **2012**, *52*, 2645.

35. Pötschke, P.; Fornes, T. D.; Paul, D. R. *Polymer* **2002**, *43*, 3247.

36. Yasmin, A.; Luo, J. J.; Daniel, I. M. *Compos. Sci. Technol.* **2006**, *66*, 1182.

37. Liu, X.; Wu, Q. *Eur. Polym. J.* **2002**, *38*, 1383.

38. Kim, I. H.; Jeong, Y. G. *J. Polym. Sci. Part B: Polym. Phys.* **2010**, *48*, 850.

39. Zhao, Y. F.; Miao, X.; Wang, S. J.; Ge, X. C.; Meng, Y. Z. *Compos. Sci. Technol.* **2007**, *67*, 2528.

40. Shu, Y.; Ye, L.; Yang, T. *J. Appl. Polym. Sci.* **2008**, *110*, 945.

41. Yasmin, A.; Daniel, I. M. *Polymer* **2004**, *45*, 8211.

42. Liu, M.; Song, G.; Yi, J.; Xu, Y. *Polym. Compos.* **2013**, *34*, 288.